1D Riemann solver involving variable horizontal density for the computation of unsteady sediment transport

C. Juez [1]; and J. Murillo [2]; and P. García-Navarro [3], M.ASCE

ABSTRACT

Intense transient shallow flows over erodible bed implies the appearance of a changing horizontal density due to the presence of sediment particles in the water layer. The lack of consideration of the variability of the bulking density of the mixture is not admissible when modeling severe types of erosional flow such as the release of a dam break wave over a sedimentary bottom. Such event can lead to significant changes in the wave hydrodynamics, since the inertia of the flow can be larger and consequently its erosion/deposition capacity can be altered. From a numerical point of view a new complex erosion/deposition source term appears. For the integration of these source terms two strategies have been explored in this work: upwind and pointwise. Hence, this work is focused on the development and validation of a novel numerical scheme based on an approximate augmented Riemann solver, where the erosion/deposition rates play an important role in the variation of mixture density. Several analytical test cases have been derived in order to validate the computational tool. The numerical predictions have also been compared against experimental data.

Keywords: Finite volume method, 1D Shallow water, variable horizontal density, bed-load transport

1 INTRODUCTION

Free surface flows with sediment transport over erodible bed in realistic situations involve

[1]LIFTEC, CSIC-Universidad de Zaragoza, C/Maria de Luna 3, 50018, Zaragoza, Spain (corresponding author). E-mail: carmelo@unizar.es.

[2]LIFTEC, CSIC-Universidad de Zaragoza, C/Maria de Luna 3, 50018, Zaragoza, Spain.

[3]LIFTEC, CSIC-Universidad de Zaragoza, C/Maria de Luna 3, 50018, Zaragoza, Spain.

transient flow and movable flow boundaries. The first step for reproducing the physics of the sediment dynamics is based on the definition of the mathematical model. Several conceptual frameworks have been proposed in a number of previous works (Armanini and Di Silvio, 1988; Lai, 1991; Armanini and Fraccarollo, 1997; Capart and Young, 1998). Among them, the model proposed by Fraccarollo and Capart (2002) was derived by means of physically consistent governing equations. The authors assumed that the flow may be stratified in a transport layer, with high sediment concentration of sediment particles and mainly governed by bed load, and an upper layer where sediment particles are transported by suspension. Moreover, the bed level was defined as the morphodynamic layer. According to Fraccarollo and Capart (2002), the bed boundary is viewed as a transition between two zones with different behaviors, the solid phase and the fluid phase. These assumptions can be used to obtain a hyperbolic system of equations with various properties which are highly desirable from a physical and computational point of view as it will be shown later.

The main drawback of this model is that it requires a number of closure equations, (Zhang et al., 2013), due to the non-continuity of velocity, shear stress and sediment concentration terms. Therefore, a one fluid layer model can be considered as a simplification, assuming that the transport layer is included within the suspension layer (Cao et al., 2002; Begnudelli et al., 2010). This one layer hypothesis allows to reduce the number of unknowns and closure equations.

Although the one layer model is a genuinely two phase flow, the system of equations has been traditionally manipulated in order to obtain an even simpler model. Hence, the sediment dynamics has often been rewritten by means of a sediment continuity equation stating that the time variation of the sediment layer in a certain volume is due to the net variation of the solid transport through the boundaries of the volume. The mathematical expression of such law is known as the Exner equation (Kalinske, 1947). Despite the fact that the Exner equation ignores the time rate of change of the sediment concentration, accurate numerical results can be obtained Murillo and García-Navarro (2010a); Xia et al. (2010);

Soares-Frazao and Zech (2010); Siviglia et al. (2013); Juez et al. (2014). Nevertheless, the Exner-based models have a strong limitation of applicability because they are based on a severe assumption regarding the concentration of sediments, i.e. mainly all the particles are moved by rolling or sorting without altering the density of the water layer. This is well known since the first works of De Vries et al. (1990) and more recently has been faced quantitatively in Garegnani et al. (2013), where a limit of 1% for the sediment concentrations has been estimated. Above this level the mixture horizontal density dynamics cannot be neglected, i.e., cannot be considered constant,is available.

Hence, when the sediment concentration transport equation is not neglected from the one layer model, the more important concern is how to deal with the extra density provided by the sediment particles. Some previous works assumed that the bulk density remains constant and equal to the water mass, Wu (2004); Wu and Wang (2007); Begnudelli et al. (2010); Canelas et al. (2013) and other works hypothesized that the volumetric concentration is given by a closure formula, as in Rosatti et al. (2007); Cao et al. (2006); Wu and Wang (2008), involving changes in the horizontal density.

This last idea, i.e. the presence of a sediment concentration in the fluid layer, should be retained when dealing with some type of erosional flows: the release of a dam break over a sedimentary bottom or an advancing flow over a poorly sorted bed. In such events, the bulking of the flow contains an important amount of eroded material and consequently, the inertia of the flow is increased, it moves faster and the erosion/deposition rates are modified. This problem is of considerable practical significance as the modeling and forecasting of massive sediment motions is a highlight issue for the safety of locations close to natural torrents, rivers or coasts. In such situations, the shallow flow assumption is well considered and for this reason, the authors disregard the possible vertical variation of the density, and restrict their attention to flows where the density changes mainly occurs over the horizontal plane.

Once a mathematical model is selected, another separate issue is the numerical scheme

used. Considering the hyperbolic nature of the depth averaged equations, Godunov type schemes are commonly used in literature. Two main families of Godunov type solvers can be found in the literature from works in the context of shallow flow over rigid bed. One family is based on extensions of the HLL scheme of Harten and Hyman (1983), that were first applied to deformable bed in Fraccarollo et al. (2003) and recently extended to 2D in Palumbo et al. (2008) following the HLLC solver of Toro (1994). On the other hand, a second family of solvers based on the Roe's approximate solver have been widely used (Hudson and Sweby, 2005; Rosatti et al., 2007; Castro Diaz et al., 2008; Liu et al., 2008). While in (Hudson and Sweby, 2005; Rosatti et al., 2007; Castro Diaz et al., 2008) computational experiments were used to analyze the performance of the numerical schemes proposed using academic test cases, in Liu et al. (2008) the proposed numerical scheme was applied to an experimental configuration. In this latter case the quality of the results was compromised by the simplicity of the closure formula, based on a calibration constant for the whole domain. It is worth noticing that, when considering several closure equations a robust and accurate numerical scheme is required. Otherwise, physical and numerical effects can be confusing, justifying a wide number of tuning parameters which in some cases are not physically based.

For our purpose the Godunov type schemes must include the presence of a variable horizontal density in their definition. Previous studies over rigid bed involving this feature were developed in Leighton et al. (2010) for 1D mesh and in Jiang et al. (2011) for 2D mesh. However, in the first work a lack of mass conservation was documented and in the second work the computational predictions were not close enough to the experimental data. In order to overcome these problems in Murillo and García-Navarro (2011) an augmented Roe solver for rigid bed was built, proving to be accurate, conservative and robust. In this work, and departing from Murillo and García-Navarro (2011), a generalized Roe numerical scheme has been defined for 1D transient flows with variable density over deformable bed. Special attention has been devoted to the linearization of the erosion/deposition source terms

since they can lead to the appearance of oscillations in the computational solution. These instabilities arise from an inadequate evaluation of the source term integral as it will be showed in further sections.

The remainder of the paper is structured as follows: first the mathematical model is described in Section 2. Section 3 is devoted to describe the numerical scheme. Section 4 displays a set of analytical and experimental test cases for validating the computational predictions. Finally, in Section 5 the conclusions of the work are summarized.

2 MATHEMATICAL MODEL AND ITS FEATURES

The relevant formulation of the model derives from the depth-averaged equation of bulk mass conservation, mixture momentum conservation and conservation of the mass of the sediment which is mobilized. That system of partial differential equations is formulated here in coupled form per unit width as follows

$$\frac{\partial \mathbf{U}}{\partial t} + \frac{\partial \mathbf{F}(\mathbf{U})}{\partial x} = \mathbf{S}(\mathbf{U}) + \mathbf{R}(\mathbf{U}) \tag{1}$$

where

$$\mathbf{U} = \begin{pmatrix} h\,r, & h\,u\,r, & h\phi \end{pmatrix}^T \tag{2}$$

are the depth-averaged conserved variables, with h representing the mixture depth, u velocity, ϕ the depth-averaged volumetric concentration of the sediment and z, the bed level. The term r is the relative density of the bulk mixture to that of the water, which is computed as follows

$$r = 1 + \Delta\phi \tag{3}$$

where $\Delta = (\rho - \rho_w)/\rho_w$ is the relative density of the sediment phase, being ρ_w the density of water and ρ the sediment density.

The fluxes are given by

$$\mathbf{F} = \left(\; hur, \quad hu^2 r + \tfrac{1}{2} g h^2 r, \quad hu\phi \; \right)^T \tag{4}$$

where g is the gravity acceleration. The source terms of the system are split in two parts. The term $\mathbf{S}$ is defined as

$$\mathbf{S} = \left(0, \; \frac{p_b}{\rho_w} - \frac{\tau_b}{\rho_w}, 0, \ldots, 0 \right)^T \tag{5}$$

with p_b and τ_b the gravity force along the bottom and the bed shear stress. The gravity is written in differential form through the bed slope

$$\frac{p_b}{\rho_w} = -ghr\frac{\partial z}{\partial x} = ghrS_0 \tag{6}$$

and the friction term is evaluated taken into account the Manning's law

$$\frac{\tau_b}{\rho_w} = ghS_f \quad S_f = \frac{n^2 u^2}{h^{4/3}} \tag{7}$$

The term $\mathbf{R}$ contains the information about the erosion/deposition source term, here called reaction term. The vector $\mathbf{R}$ is written in a 1D general form as follows:

$$\mathbf{R} = (\Delta R, 0, R)^T \tag{8}$$

The reaction terms are the responsible of the material exchange between the bed and fluid layers. Hence, the bed variation is written as,

$$\frac{\partial z}{\partial t} = -\frac{R}{(1-p)} \tag{9}$$

being p the porosity of the sediment. It is worth remarking that the maximum sediment concentration allowed in the flow is given by $1-p$. Additionally, the term R can be evaluated

by means of several ways, as described in Wu (2007). It assumes the same settling velocity for the deposition and for the entrainment,

$$R = \omega_s \left(\phi_* - \phi \right) \tag{10}$$

where the term ϕ_* is the equilibrium concentration, which is obtained through a solid transport discharge law such as Grass (1981); Meyer-Peter and Müller (1948); Smart (1984). The term ϕ contains the information about the suspension sediment quantity which is transported within the fluid layer. Both concentrations take in consideration the presence of the settling velocity, ω_s. This non-equilibrium formula, 10, which drives the transport rate towards its equilibrium capacity, has been used for computing all the tests in further sections.

Focusing on the characteristics of system (1), this system is time dependent, non linear, and contains source terms. If it is assumed that the advective terms are dominant then the system has an hyperbolic character. Therefore, the mathematical properties of the system of equations include the existence of a Jacobian matrix, $\mathbf{J}$, where all the eigenvalues are real (Murillo et al., 2012). This information is relevant for making use of the first order Roe's numerical scheme described in the next section.

3 FINITE VOLUME MODEL

In order to obtain a numerical solution of system (1) the computational domain is divided in cells of equal length sized Δx. The interval of the i-th cell is defined by $[x_{i-1/2}, x_{i+1/2}]$ where $x_{i+1/2} = i\Delta x$ and the location of the cell center x_i is defined by $(i-1/2)\Delta x$. Δt is the time step and $t^n = n\Delta t$ is a generic time. Considering the traditional notation we indicate with $\mathbf{U}_i^n$ the cell-average value of the solution $\mathbf{U}(x,t)$ for the ith cell at time t^n:

$$\mathbf{U}_i^n = \frac{1}{\Delta x} \int_{x_{i-1/2}}^{x_{i+1/2}} \mathbf{U}(x, t^n) dx \tag{11}$$

$\mathbf{U}_i^n$ is therefore a piecewise constant approximation of the solution at time t^n of the conserved variables.

Thanks to the piecewise constant data the Godunov method, (Godunov, 1959), is applied and consequently the theory of Riemann Problems (RP) can be considered. The advantage of using this theory is clear: it is not necessary to know the exact solution for the internal wave description of the RP and hence, a set of linearized approximate solutions (also called weak solutions) can be built.

On the other hand, within the framework of the Godunov methods two common strategies are used for updating the conserved variables: the upwind and the pointwise technique. The upwind philosophy has been traditionally retained for the building of the numerical fluxes. Contrary, the pointwise technique has been used for the integration of the source terms. However, in Murillo and García-Navarro (2010b) it was developed an original idea about the presence of steady state waves in the definition of the wave structure of each RP. Hence, a steady jump discontinuity is considered to represent each source term in order to incorporate this information into the classical wave description for building the fluxes. This typology of augmented approximate Riemann solvers has been used recently Murillo and García-Navarro (2010a, 2011); Murillo et al. (2012); Juez et al. (2014) leading to encouraging results.

Departing from the Reduced Godunov first order method proposed in Murillo et al. (2012), we consider the appearance of a new erosion/deposition source term into the numerical scheme. Two strategies are considered for the integration of this source term: upwind and pointwise. One of the purposes of this work is to clearly identify the possibilities of each type of discretization.

Godunov Method and upwind integration of the erosion/deposition source term

Following the Reduced Godunov first order method proposed in Murillo et al. (2012), system (1) is split in two types of variables. The first are the reduced set of hydrodynamic conserved variables referred as $\mathbf{U}^r = (hr, hur)$, which are updated using a splitting technique

$$\mathbf{U}_i^{r,n+1} = \mathbf{U}_i^{r,n} - (\delta\mathbf{M}_{i+1/2}^- + \delta\mathbf{M}_{i-1/2}^+)\frac{\Delta t}{\Delta x} \tag{12}$$

where the matrices $\mathbf{M}$ contain information about the fluxes and source terms. The term Δt

is the timestep chosen for updating the variables and Δx is the length between neighboring cells which can vary along the computational domain

Additionally, the conserved sediment concentration, $h\phi$, is updated taking into account the sign of the mixture mass discharge which crosses each edge of each cell, $q_m^{\downarrow}$,

$$h\phi_i^{n+1} = h\phi_i^n - (q_{phi})^{\downarrow}\frac{\Delta t}{\Delta x} \tag{13}$$

where

$$(q_{phi})^{\downarrow} = \begin{cases} \frac{q_m^{-\downarrow}}{r_i}\phi_i & \text{if} \quad q_m^{\downarrow} > 0 \\ (\frac{q_m^{+\downarrow}}{r_{i+1}}\phi_{i+1} - \bar{R}_{i+1/2}) & \text{if} \quad q_m^{\downarrow} < 0 \end{cases} \tag{14}$$

and as it can be observed, the erosion/deposition term, R, plays its upwinding role according to the sign of the mixture discharge.

Finally, the bed level, z, is updated as

$$z_i^{n+1} = z_i^n - (q_z)^{\downarrow}\frac{\Delta t}{\Delta x} \tag{15}$$

where

$$(q_z)^{\downarrow} = \begin{cases} 0 & \text{if} \quad q_m^{\downarrow} > 0 \\ \bar{R}_{i+1/2} & \text{if} \quad q_m^{\downarrow} < 0 \end{cases} \tag{16}$$

Godunov Method and pointwise integration of the erosion/deposition source term

In this case, the erosion/deposition source term is not considered when building the matrices $\mathbf{M}$ and it is pointwise integrated. Hence, the numerical scheme is built as follows

$$\mathbf{U}_i^{n+1} = \mathbf{U}_i^n - (\delta\mathbf{M}_{i+1/2}^- + \delta\mathbf{M}_{i-1/2}^+)\frac{\Delta t}{\Delta x} + \mathbf{R}_i^n\Delta t \quad with \quad \mathbf{R}_i = \mathbf{R}_i^n \tag{17}$$

where $\mathbf{U}$ is the complete set of conserved variables, and the bed level is updated as

$$z_i^{n+1} = z_i^n - R_i^n \Delta t \quad with \quad R_i = R_i^n \tag{18}$$

Finally, with both strategies, upwind (12,15) and pointwise (17,18) the time step Δt is taken small enough so that there is no interaction of waves from the k neighboring RPs, i.e., the CFL (Courant Friedrichs Lewy) condition (Leveque, 2002; Murillo et al., 2012) is considered.

4 RESULTS

This section has been divided in two parts. The first part is devoted to perform a numerical assessment of the erosion/deposition source term discretization: pointwise and upwind. In the second part, the numerical predictions are compared with respect to experimental data and also some numerical experiments are considered.

4.1 Numerical test cases

These test cases are motivated by the utmost importance of the discretization of the erosion/deposition source term: pointwise or upwind. It must be stressed that an accurate behavior of this reaction term allows to state a starting point for studying the bed level evolution. The examples are chosen to consider different hydrodynamic and morphodynamic combinations. The geometric framework of all them is the same: a straight, 12 meters long channel. For each test case a variable bed slope within the channel is derived. For this reason the bed slope and bed level evolution along the longitudinal direction are plotted for each test studied. Numerical simulations have been carried out using CFL=1.0 with Δx=0.1 m and ω_s=0.01 m/s.

Test 1

Test case 1 lies in a combination of a complex bottom definition, a steady flow, $q = hu$ =0.02 m^2/s, frictionless assumption, and also considering that the erosion/deposition term only implies deposition process, i.e., an effective negative reaction term. For this first

case, the bed level is not updated and only the reaction term evolution is studied.

An analytical solution is derived in order to be compared with the numerical results. Firstly, the sediment concentration profile along the domain is obtained from the sediment transport equation, imposing steady flow and only deposition process, i.e., $\phi^*= 0$

$$\frac{dhu\phi}{dx} = R \qquad with \quad R = \omega_s \left(\phi^* - \phi\right) \tag{19}$$

$$\frac{dhu\phi}{dx} = -\omega_s \phi \tag{20}$$

which allows to express the sediment concentration variation along the domain as

$$\frac{d\phi}{dx} = -\frac{\omega_s}{q}\phi \tag{21}$$

Now considering the 1D frictionless momentum equation, which states

$$\frac{d}{dx}\left(r\frac{q^2}{h} + \frac{g}{2}h^2 r\right) = ghr\left(\frac{-dz}{dx}\right) \tag{22}$$

applying the chain rule to the left side

$$r\frac{d}{dx}\left(\frac{q^2}{h} + g\frac{h^2}{2}\right) + \left(\frac{q^2}{h} + g\frac{h^2}{2}\right)\frac{dr}{dx} = ghr\left(\frac{-dz}{dx}\right) \tag{23}$$

and considering $r = 1 + \Delta\phi$ the following equation is obtained

$$(1+\Delta\phi)\frac{dh}{dx}\left(gh - \frac{q^2}{h}\right) + \left(\frac{q^2}{h} + g\frac{h^2}{2}\right)\Delta\frac{d\phi}{dx} = gh(1+\Delta\phi)\left(\frac{-dz}{dx}\right) \tag{24}$$

Substituting (21) in (24) and rearranging the resulting equation yields to

$$\frac{dz}{dx} = \frac{dh}{dx}\left(\frac{u^2}{gh} - 1\right) + \frac{(q^2/h + gh^2/2)}{gh}\frac{\Delta}{1+\Delta\phi}\left(\frac{\omega_s\phi}{q}\right) \tag{25}$$

where the sediment concentration, ϕ, is obtained by integrating (21),

$$\phi(x) = \phi_0 \exp\left(-\frac{\omega_s(x - x_0)}{q}\right) \tag{26}$$

and it is considered that the initial sediment concentration in the fluid layer is $\phi_0 = 0.5$. Note that equation (25), neglecting the terms associated to the variable density and considering the Froude number ($Fr = u/\sqrt{gh}$), is in fact a simple-wave equation

$$\frac{dz}{dx} = \frac{dh}{dx}\left(Fr^2 - 1\right) \tag{27}$$

Since it is mandatory to know the function of $h(x)$ in (25) to obtain its derivative, a linear water level, $h(x) = 0.1 + 0.01x$ is assumed in this test case. Figure 1 shows the resulting bed slope obtained. As it is observed, the presence of the variable horizontal density in (25), i.e., the term $\frac{\Delta}{1+\Delta\phi}$, yields to obtain a non-uniform bed slope along the domain.

Figure 2 displays the exact and numerical solution after 500 s for the water level surface, the unit flow discharge and the sediment concentration when using the pointwise and the upwind approach. Despite providing both approaches accurate results, only the upwind discretization is able to reach a stationary flow within the domain. When plotting the sediment concentration evolution and the absolute error (the difference between the numerical and experimental solution) associated to each approach, Figure 3, it is clear that the pointwise approach introduces a larger error than the upwind scheme. Since the change in the bed slope is bigger in the first meters of the domain, Figure 1, it can be justified that the maximum error in the sediment concentration is also located in that zone.

Test 2

This test case is based on a steady flow, $q = hu$ =0.2 m^2/s, over a complex bottom including a friction term ($n = 0.00165 sm^{-1/3}$) and an equilibrium sediment stage is simulated by imposing $R = 0$. This implies that no exchange exits between the bed and the upper layers of the flow, i.e., the erosion/deposition processes are well balanced. The initial sediment

concentration assumed for this test case is $\phi_0 = 0.4$.

Returning to the 1D sediment transport equation and imposing the conditions above explained the restriction which yields is that the sediment concentration is constant along the domain,

$$\frac{d\phi}{dx} = 0 \tag{28}$$

Assuming $R = \omega_s (\phi_* - \phi) = 0$, it implies that $\phi = \phi_*$ and also, since there is a sediment equilibrium, $\phi = \phi_* = \phi_0 = 0.4$. If it is considered that the solid discharge can be computed by means of the Grass law (Kalinske, 1947). This formula is based on a power velocity law and on a constant calibration parameter. Due to its simplicity, it is convenient for mathematical manipulation,

$$q_s = A_g u^3 \tag{29}$$

and considering that the solid discharge flow can be also written as

$$q_s = hu\phi_* \tag{30}$$

then, the A_g factor must vary along the domain following this relation,

$$A_g = \left(\frac{\phi_*}{q^2}\right) h^3 \tag{31}$$

where ϕ_*/q^2.

Bearing in mind condition derived in (28) and working with the momentum equation the resulting bed level variation is the same as the one obtained in (27)

$$\frac{dz}{dx} = \frac{dh}{dx}\left(Fr^2 - 1\right) - S_f \tag{32}$$

Figure 4 displays the resulting bed slope and bed level along the domain.

The analytical solution is compared with the numerical one in Figure 5 after 200 s. The upwind approach provides accurate results whereas the pointwise approach leads to erroneous ones. It must be stressed that since the erosion/deposition term is null in this situation, the bed level must keep invariable in time. This situation is only achieved when using the upwind approach, since no oscillations in the surface level are observed. Figure 6 shows the sediment concentration computed with every approach. Again, the sediment concentration is only accurately captured with the upwind technique. With the pointwise approach since it is decreasing, i.e. a deposition process is occurring, the bed level is erroneously increasing.

Test 3

Test case 3 is one step more in the complexity of the exact and numerical solution studied. A steady flow stage, $q = hu$ =0.2 m^2/s, with a variable bottom, including friction term and a reaction term which incorporates both deposition and erosion process are considered. With these assumptions the advection equation for the sediment concentration is written neglecting the temporal term and moving the water discharge, $q = hu$ =, which is constant, to the right side of the equation

$$\frac{d\phi}{dx} = \frac{\omega_s}{q}(\phi_* - \phi) \tag{33}$$

The equilibrium concentration in (33), ϕ_*, is obtained when linking the Grass equation, (29), and the equation for the solid discharge, q_s, (30) as in previous test

$$\phi_* = A_g \frac{q^2}{h^3} \tag{34}$$

For this particular case, the A_g is supposed constant for all the domain and equal to 0.1. Following the same procedure as in the previous test case, the bed variation along the x coordinate can be written as

$$\frac{dz}{dx} = \frac{dh}{dx}\left(\frac{u^2}{gh} - 1\right) + \frac{(q^2/h + gh^2/2)}{gh}\frac{\Delta}{1+\Delta\phi}\left(\frac{\omega_s\phi}{q} - \frac{A_g\omega_s q}{h^3}\right) - S_f \tag{35}$$

where S_f is the friction term, calculated in terms of the Manning-Strickler's coefficient, $n = 0.00165 s m^{-1/3}$. The sediment concentration is obtained after integrating (33)

$$\phi(x) = \phi_* - (\phi_* - \phi_0) \exp - \frac{\omega_s (x - x_0)}{q} \tag{36}$$

and it is considered that the initial sediment concentration in the fluid layer is $\phi_0 = 0.5$.

Figure 7 displays the bed slope obtained from equation (35) and the resulting bed level. A non uniform value for the bed slope along the x coordinate is generated due to the relative density: regarding (35,36) the non-linearity of the bed slope is due to the sediment concentration profile which evolves exponentially along the x coordinate.

Figure 8 shows numerical solution for the water level and the bed level using the upwind and pointwise approaches. The upwind discretization achieves a linear water level whereas the pointwise approach predicts oscillations in the computed solution. Same conclusions arise when observing the bed level. Note that the bed level has been increased with respect to the initial configuration considered: this implies that the overall sign of the reaction term has been negative and the sedimentation process has been dominant. Figure 9 displays the unit flow discharge and the sediment concentration along the domain. A steady stage is reached when employing the upwinding technique. The sediment concentration evolution is also presented and only a monotonic distribution of the concentration is obtained with the upwind approach.

Test 4

The particularity of this test is the fact that a dominant phenomenon of erosion/deposition is alternated within the domain. It is based on the same equations (35,36) and hypothesis described in test case 3 (steady flow with $q = hu$ =0.2 m^2/s, friction term with $n = 0.00165 s m^{-1/3}$ and Grass law for sediment discharge with $A_g = 0.1$ constant for all the domain), except in the initial concentration considered, which in this case is equal to $\phi_0 = 0.15$. This means that the reaction term has not a uniform sign when the steady state is reached, Figure 10. The resulting bed slope and bed level evolution, keeping present (35)

306 and (36), are shown in Figure 11.

307 Figure 12 depicts the exact and numerical solution for the water level surface and the unit
308 discharge flow after 1200 s when using the pointwise approach and the upwind approach.
309 At first glance, similar and accurate results are provided. However, when analyzing the unit
310 flow discharge the pointwise approach is not able to guarantee an uniform flow. In Figure 13
311 the sediment concentration evolution, exact and numerical, and the error associated to each
312 approach is presented. The upwinding technique is the more accurate approach although
313 differences are not so significant as in the previous test cases.

314 **4.2 Experimental 1D dam break over deformable bed**

315 Experimental data are used to validate the models under realistic conditions. The hydro-
316 morphodynamic changes which take place during the dam break in a rectangular straight
317 channel are numerically reproduced in this section. These experiments were performed in a
318 flume designed at the Université Catholique de Louvain (Belgium) in the Civil Engineering
319 Department by Spinewine and Zech (2007). The flume had a length of 6 m, 3 m on both
320 sides of a central gate simulating an idealized dam. The channel width was set constant and
321 equal to 25 cm. The bed material was uniform coarse sand with the following properties:
322 particle sizes ranging from 1.2 to 2.4 mm, with $d_{50} = 1.82$ mm, density $\rho_s = 2683$ kg m^{-3}, a
323 friction angle $\varphi = 30^o$, negligible cohesion, porosity $p = 0.47$. The Manning roughness factor
324 was estimated to be $n = 0.0165$ sm$^{-1/3}$. Upstream and downstream the gate different levels
325 of clean water, i.e., $\phi_0 = 0$, and sediment were imposed, Figure 14.

326 From Spinewine and Zech (2007) two experimental configurations have been chosen for
327 validating the numerical predictions. The first experiment is based on a dam break which
328 advances over dry bed. From a physical point of view it is expected to find peaks of sediment
329 concentration over the step and in the front of the wave. The ability of the numerical
330 scheme for avoiding numerical instabilities in that areas deserves to be tested. The second
331 configuration addressed is a dam break over a wet bottom. For this test case, it is important
332 to verify if the hydraulic jump, which is generated downstream the step, is well tracked

despite of the sediment particles which are incorporated to the fluid layer and which modify the resulting bulking density.

Numerical simulations have been performed considering a CFL = 1.0, the upwind technique for the discretization of the reaction term and a domain fully deformable. The closure equation employed for computing the solid discharge is the Smart formula (Smart, 1984) fixed by Juez et al. (2013). Equaling this empirical solid discharge with (30) it is obtained the ϕ_* value for lumping it in (10). The upwind discretization has been chosen for the integration of the erosion/deposition term since from the previous numerical test cases has been inferred that it provides the more accurate and reliable predictions.

Test A

The initial conditions of water and sediment were: upstream the gate $h_w = 0.35$ m and $z_s = 0.1$ m and downstream the gate h_w=z_s=0 m.

Figure 15 displays computed results and experimental data at several times for the surface level and bed level. The flow develops leading to a left moving rarefaction wave ending in a front wave dominated by friction and erosion. The numerical scheme is able to handle accurately this kind of bed discontinuity, tracking the water level surface and redrawing correctly the bed level. Neither numerical oscillations nor negative water depth appears despite of the presence of both rarefaction wave and advance front wave over wet/dry boundaries. Considering that the numerical scheme is conservative, slight differences among measured and computational data are expected to be produced by the lack of an infiltration parameter in the numerical model.

Figure 16 displays the temporal and spatial evolution of the sediment concentration along the domain. The maximum sediment concentration evolves with the advance wave as it is a wet/dry situation. Moreover the computed solution shows a monotonic distribution without numerical instabilities. It is also remarkable the fact that a second peak in the sediment concentration appears at the bottom step, as in that zone the erosion/sedimentation process

has a bigger influence than in the rest of the domain.

This experiment was already numerically reproduced by the authors in Juez et al. (2014) assuming a constant value for the density. When comparing both results, the main differences appear at the bed-step area and in the front zone of the dam break, where the sediment concentration becomes more relevant, i.e., more than 1%. Computing and comparing the absolute error percentage, i.e. the difference between the numerical and experimental, it yields to obtain on average a 13% less error when assuming a variable horizontal density within the equations.

Additionally, and in order to reinforce the importance of taking density variations into account this experiment has been reproduced assuming that the initial water depth has a sediment concentration equal to $\phi_0 = 0.2$. Figure 17 displays the surface and bed level evolution: due to the presence of an initial amount of sediments in the bulk density the inertia of the flow is larger when comparing with clean water and consequently it moves faster. On the other hand, in Figure 18 the sediment concentration is plotted at several times. When comparing with the clean water test case it can be observed how the peak erosion is smaller since the erosion capacity of the flow is decreased by the amount of sediment that is yet being transported.

Test B

The initial conditions of water and sediment were: upwards the gate $h_w = 0.35$ m and $z_s = 0.1$ m and downwards the gate $h_w = 0.1$ m and $z_s = 0$ m.

The water surface and bed level temporal evolution are plotted in Figure 19. A moving rarefaction wave is propagated upstream the step and an hydraulic jump, located in the step area, migrates downstream ending up with a right moving shock. Slight differences are found among experimental data and computational results and they can be attributed to the fast energy dissipation which is occurring in the hydraulic jump. In Figure 20 the sediment concentration is displayed and the peak of the curve is located in the vicinity of bed step

which is the place where the erosion process is dominant. It is worth notifying the fact that in this case since there is a no wet/dry situation, the maximum sediment concentration value is less than in the previous case.

Newly, a comparison in terms of absolute error percentage is performed bearing in mind the results with constant density previously studied in Juez et al. (2014). For this test case, the results displayed in this work provide a 9.5% less error. Thanks to the extra density which is provided due to erosion, the hydrodynamic/morphological evolution of the test case is described with a better level of accuracy.

5 CONCLUSIONS

A 1D numerical scheme for shallow flows over mobile beds with variable horizontal density has been detailed. It is written under the form of a finite volume method based on a Roe type solver and using the splitting technique and the Reduced Godunov scheme. The explicit scheme has shown to be robust and stable, always controlled by the CFL stability condition.

The numerical technique has been validated using exact and experimental test cases. In the academic test cases it has been stated how the upwind approach provides physical and accurate results whereas the pointwise discretization of the reaction terms leads to oscillatory solutions where a steady state is not achieved.

In the experimental test cases the advance front celerity evolving over dry and wet bed has been well captured along the dam break. The erosion-deposition rates are also well tracked leading to accurate computed results against the laboratory data. With respect to the temporal and spatial sediment concentration variation it is worth noticing that despite not having experimental data of this feature during the experiment, the numerical solution shows a monotone evolution, neglecting the presence of unphysical oscillations. In addition, the peaks of concentration can be well understood, as they appear in the front of moving wave in the dry case and over the favorable step in both tests. When considering an initial high sediment concentration, the behavior of the dam break is faster in comparison with the clean water test case. The bulking density plays an important role on the hydrodynamic and morphodynamic patterns. Hence, the necessity for a numerical tool which incorporates the relative density features is justified.

6 ACKNOWLEDGEMENT

This work has been partially funded by the Spanish Ministry of Science and Technology under research projects CGL2011-28590.

REFERENCES

Armanini, A. and Di Silvio, G. (1988). "A one-dimensional model for the transport of a sediment mixture in non-equilibrium conditions." *Journal of Hydraulic Research*, 26, 275–292.

Armanini, A. and Fraccarollo, L. (1997). "Critical conditions for debris flows." *Proc. First Intl. Conf. on Debris-Flow Hazards Mitigation*, -, 434–443.

Begnudelli, L., Valiani, A., and Sanders, B. F. (2010). "A balanced treatment of secondary currents, turbulence and dispersion in a depth-integrated hydrodynamic and bed deformation model for channel bends." *Advances in Water Resources*, 33, 17–33.

Canelas, R., Murillo, J., and Ferreira, R. (2013). "Two-dimensional depth-averaged modelling of dam-break flows over mobile beds." *Journal of Hydraulic Research*, 51(4), 392–407.

Cao, Z., Day, R., and Egashira, S. (2002). "Coupled and decoupled numerical modeling of flow and morphological evolution in alluvial rivers." *Journal of Hydraulic Engineering*, 128, 306–321.

Cao, Z., Pender, G., and Carling, P. (2006). "Shallow water hydrodynamic models for hyperconcentrated sediment-laden flows over erodible bed." *Advances in Water Resources*, 29(4), 546–557.

Capart, H. and Young, D. (1998). "Formation of a jump by the dam-break wave over a granular bed." *Journal of Fluid Mechanics* , 372, 165–187.

Castro Diaz, M., Fernandez Nieto, E., and Ferreiro, A. (2008). "Sediment transport models in shallow water equations and numerical approach by high order finite volume methods." *Journal of Computational Fluids*, 37, 299–316.

439 De Vries, M., Klaassen, G., and Struiksma, N. (1990). "On the use of movable-bed models
440 for river problems: a state of the art." *International Journal of Sediment Research*, 5(1),
441 35–47.

442 Fraccarollo, L. and Capart, H. (2002). "Riemann Wave description of erosional dam-break
443 flows." *Journal of Fluid Mechanics*, 461, 115–133.

444 Fraccarollo, L., Capart, H., and Zech, Y. (2003). "A Godunov method for the computation of
445 erosional shallow water transients." *International Journal of Numerical Methods in Fluids*,
446 41, 951–976.

447 Garegnani, G., Rosatti, G., and Bonaventura, L. (2013). "On the range of validity of the
448 Exner-based models for mobile-bed river flow simulations." *Journal of Hydraulic Research*,
449 51(4), 380–391.

450 Godunov, S. (1959). "A difference method for numerical calculation of discontinuous solutins
451 of the equations of hydrodynamics." *Mat. Sb.*, 47, 271–306.

452 Grass, A. (1981). *Sediments transport by waves and currents*. SERC London Cent. Mar.
453 Technol, Report No. FL.

454 Harten, A. and Hyman, J. M. (1983). "Self adjusting grid methods for one-dimensional
455 hyperbolic conservation laws." *Journal of Computational Physics*, 50, 235–269.

456 Hudson, J. and Sweby, P. K. (2005). "A high-resolution scheme for the equations governing
457 2D bed-load sediment transport." *International Journal of Numerical Methods in Fluids*,
458 47, 1085–1091.

459 Jiang, L., Borthwick, A. G. L., Kramer, T., and Jozsa, J. (2011). "Variable density bore in-
460 teractions with block obstacles." *International Journal of Computational Fluid Dynamics*,
461 25(4), 223–237.

462 Juez, C., Murillo, J., and García-Navarro, P. (2013). "2D simulation of granular flow over ir-
463 regular steep slopes using global and local coordinates." *Journal of Computational Physics*,
464 255, 166–204.

465 Juez, C., Murillo, J., and García-Navarro, P. (2014). "A 2D weakly-coupled and efficient nu-
466 merical model for transient shallow flow and movable bed." *Advances in Water Resources*,
467 71, 93–109.

468 Kalinske, A. (1947). "Movement of sediment as bed load in rivers." *Trans. AGU* , 28, 615–
469 620.

470 Lai, C. (1991). "Modelling alluvial channel flow by multimode characteristic method." *Jour-*
471 *nal of Hydraulic Engineering*, 117, 32–53.

472 Leighton, F. Z., Borthwick, A. G. L., and Taylor, P. H. (2010). "1D Numerical modeling
473 of shallow flows with variable horizontal density." *International Journal For Numerical*
474 *Methods in Fluids*, 62, 1209–1231.

475 Leveque, R. (2002). *Finite Volume Methods for Hyperbolic Problems*. Cambridge University
476 Press, New York.

477 Liu, X., Landry, B., and García, M. (2008). "Two-dimensional scour simulations based
478 on coupled model of shallow water equations and sediment transport on unstructured
479 meshes." *Coastal Engineering*, 55, 800–810.

480 Meyer-Peter, E. and Müller, R. (1948). *In: Report on the 2nd Meeting International Asso-*
481 *ciation Hydraulic Structure Research*. Stockholm, Sweden.

482 Murillo, J. and García-Navarro, P. (2010a). "An Exner-based coupled model for two-
483 dimensional transient flow over erodible bed." *Journal of Computational Physics*, 229,
484 8704–8732.

485 Murillo, J. and García-Navarro, P. (2010b). "Weak solutions for partial differential equations
486 with source terms: Application to the shallow water equations." *Journal of Computational*
487 *Physics*, 229, 4327–4368.

488 Murillo, J. and García-Navarro, P. (2011). "Improved Riemann solvers for complex transport
489 in two-dimensional unsteady shallow flow." *Journal of Computational Physics*, 230, 7202–
490 7239.

491 Murillo, J., Latorre, B., and García-Navarro, P. (2012). "A Riemann solver for unsteady
492 computation of 2D shallow flows with variable density." *Journal of Computational Physics*,
493 231:4, 1963–2001.

494 Palumbo, A., Soares-Frazao, S., Goutiere, L., Pianese, D., and Zech, Y. (2008). *Proc., River*
495 *Flow 2008 International Conference on Fluvial hydraulics, Cesme.*

496 Rosatti, G., Murillo, J., and Fraccarollo, L. (2007). "Generalized Roe schemes for 1D two-
497 phase, free-surface flows over a mobile bed." *Journal of Computational Physics*, 54, 543–
498 590.

499 Siviglia, A., Stecca, G., Vanzo, D., Zolezzi, G., Toro, E., and Tubino, M. (2013). "Numer-
500 ical modelling of two-dimensional morphodynamics with applications to river bars and
501 bifurcations." *Advances in Water Resources*, 52, 243–260.

502 Smart, G. (1984). "Sediment transport formula for steep channels." *Journal of Hydraulic*
503 *Engineering*, 3, 267–276.

504 Soares-Frazao, S. and Zech, Y. (2010). "HLLC scheme with novel wave-speed estimators
505 appropiate for two-dimensional shallow-water flow on erodible bed." *International Journal*
506 *of Numerical Methods in Fluids*, 66(8), 1019–1036.

507 Spinewine, B. and Zech, Y. (2007). "Small-scale laboratory dam-break waves on movable
508 beds." *Journal of Hydraulic Research*, 45, 73–86.

509 Toro, E. (1994). "Restoration of the contact surface in the HLL Riemann solver." *Shock*
510 *Waves*.

511 Wu, W. (2004). "Depth-Averaged Two-Dimensional Numerical Modeling of Unsteady Flow
512 and Nonuniform Sediment Transport in Open Channels." *Journal of Hydraulic Engineer-*
513 *ing*, 130(10), 1013–1024.

514 Wu, W. (2007). *Computational river dynamics*. Taylor and Francis.

515 Wu, W. and Wang, S. (2007). "One-Dimensional Modeling of Dam-Break Flow over Movable
516 Beds." *Journal of Hydraulic Engineering*, 133, 48–58.

517 Wu, W. and Wang, S. (2008). "One-dimensional explicit finite-volume model for sediment
518 transport with transient flows over movable beds." *Journal of Hydraulic Research*, 46,
519 87–98.

520 Xia, J., Lin, B., Falconer, R., and Wang, G. (2010). "Modelling Dam-break Flows over
521 Mobile Beds using a 2D Coupled Approach." *Advances in Water Resources*, 33, 171–183.

522 Zhang, S., Duan, J. G., and Strelkoff, T. S. (2013). "Grain-scale nonequilibrium sediment
523 transport model for unsteady flow." *Journal of Hydraulic Engineering*, 139, 22–36.

APPENDIX I. NOTATION

The following symbols are used in this paper:

x = spatial coordinate (m);

t = time (s);

h = water depth (m);

hu = unit water discharge (m^2/s);

u = depth averaged velocity (m/s)

r = relative density of the bulk mixture (-)

Δ = relative density of the sediment (-)

ϕ = sediment concentration (-)

ϕ_* = equilibrium sediment concentration (-)

z = bed level (m)

n = Manning coefficient ($sm^{-1/3}$);

p = sediment porosity (-)

P_b = pressure force (m^2/s^2)

ρ = sediment density (kg/m^3)

ρ_w = water density (kg/m^3)

g = gravity acceleration (m/s^2)

ω_s = settling velocity (m/s)

Δt = timestep (s)

Δx = length between neighboring cells (m)

$q_m^{\downarrow}$ = mixture discharge crossing the edge of a cell (m^2/s)

q = unit water discharge (m^2/s); and

A_g = parameter of the Grass formulation (s^2/m).

List of Figures

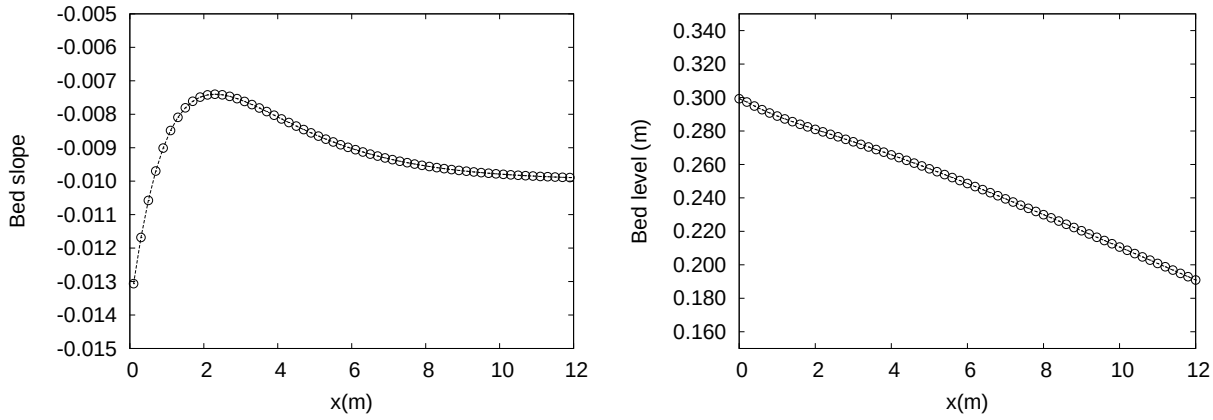

FIG. 1. Test case 1. Bed slope and bed level along the x coordinate

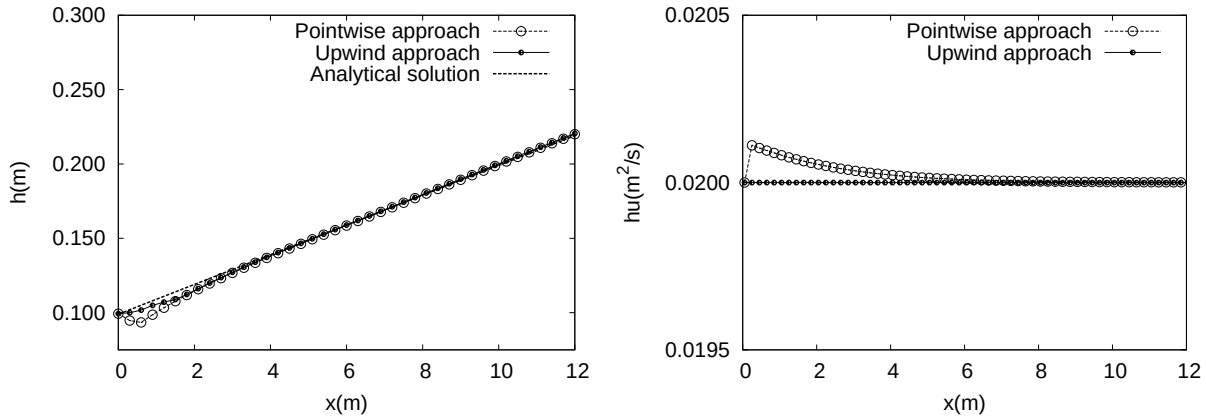

FIG. 2. Test case 1. Numerical solutions for the water level surface and unit discharge flow at t = 500 s when using the pointwise approach and the upwind approach

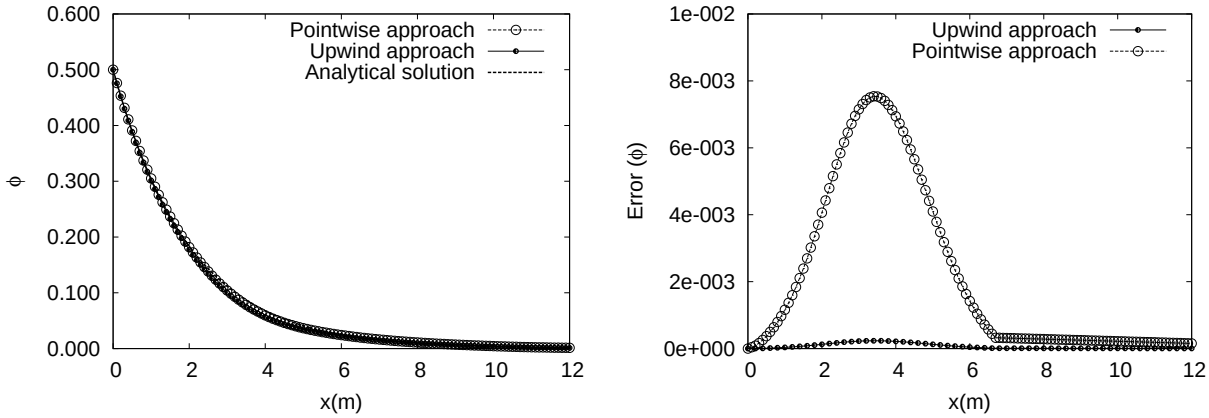

FIG. 3. Test case 1. Sediment concentration and absolute concentration error along the x coordinate at t = 500 s when using the pointwise approach and the upwind approach

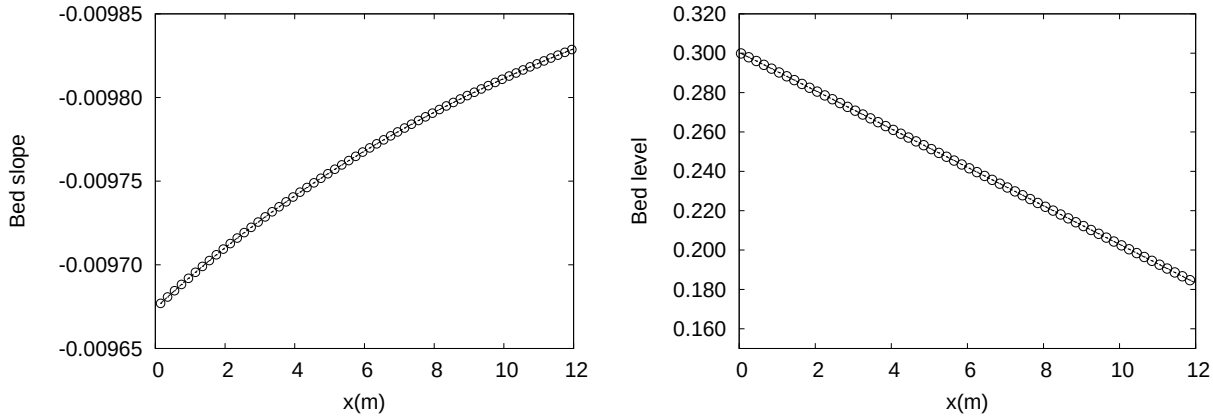

FIG. 4. Test case 2. Bed slope and bed level along the x coordinate

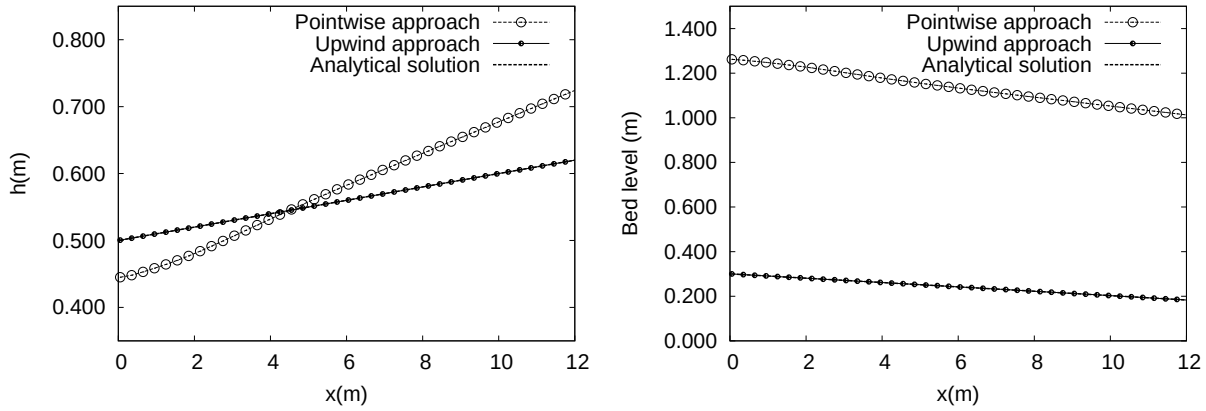

FIG. 5. Test case 2. Numerical solutions for the water level surface and bed level at t = 200 s when using the pointwise approach and the upwind approach

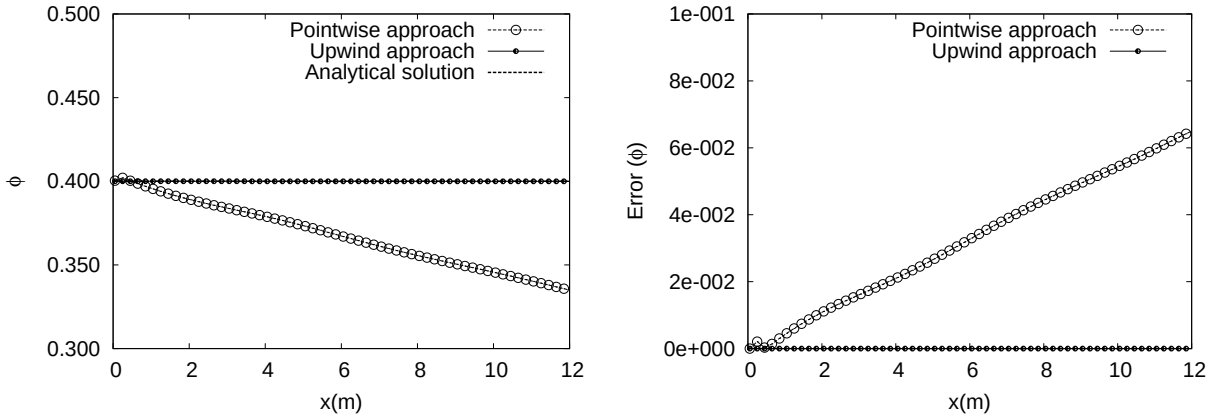

FIG. 6. Test case 2. Sediment concentration and absolute concentration error along the x coordinate at t = 200 s when using the pointwise approach and the upwind approach

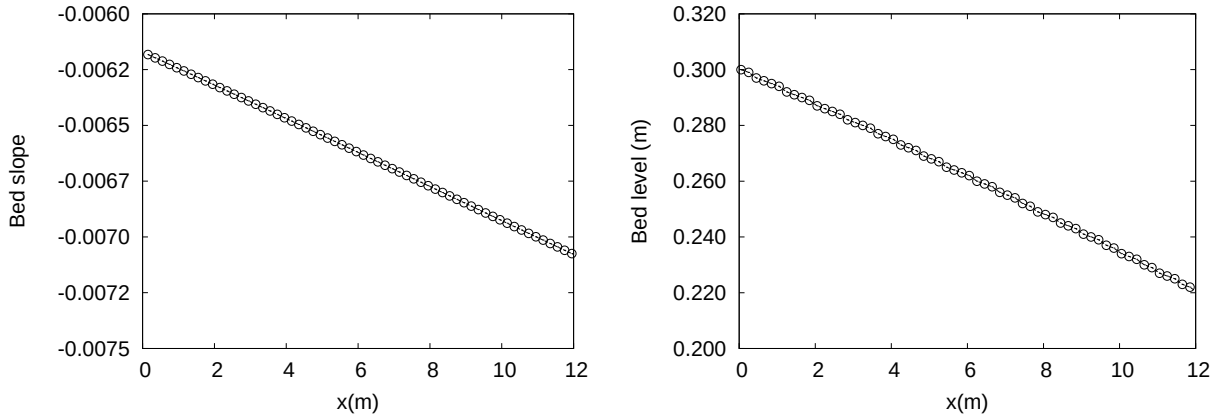

FIG. 7. Test case 3. Bed slope and bed level along the x coordinate

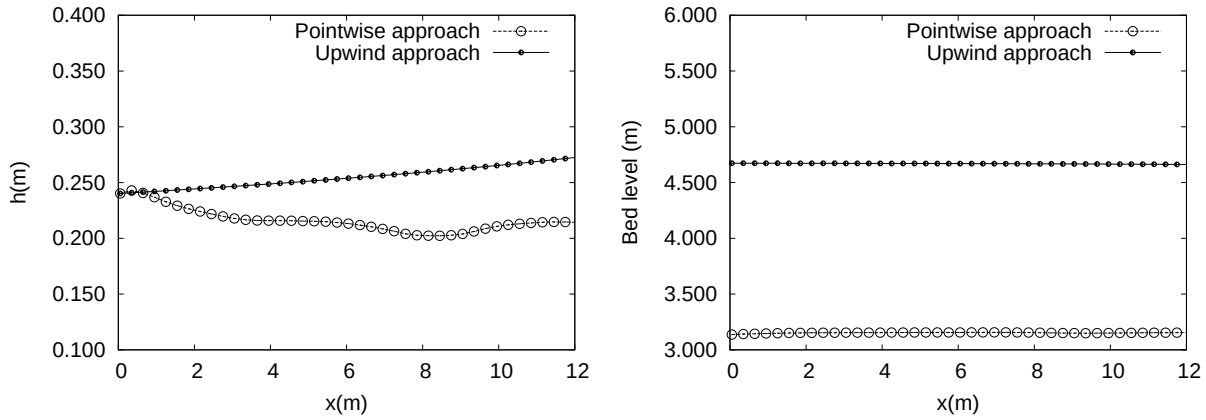

FIG. 8. Test case 3. Numerical solutions for the water level and bed level at $t = 1200$ s when using the pointwise approach and the upwind approach

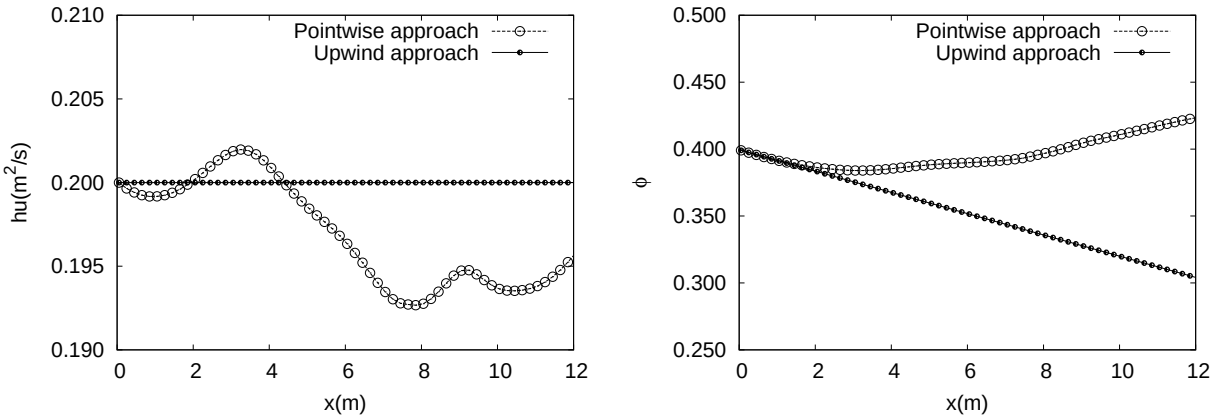

FIG. 9. Test case 3. Unit discharge flow and sediment concentration along the x coordinate at $t = 1200$ s when using the pointwise approach and the upwind approach

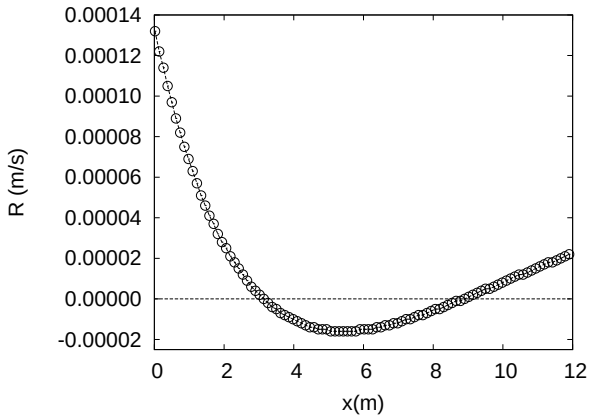

FIG. 10. Test case 4. Reaction term, $R = \omega_s(\phi_* - \phi)$, along the x coordinate

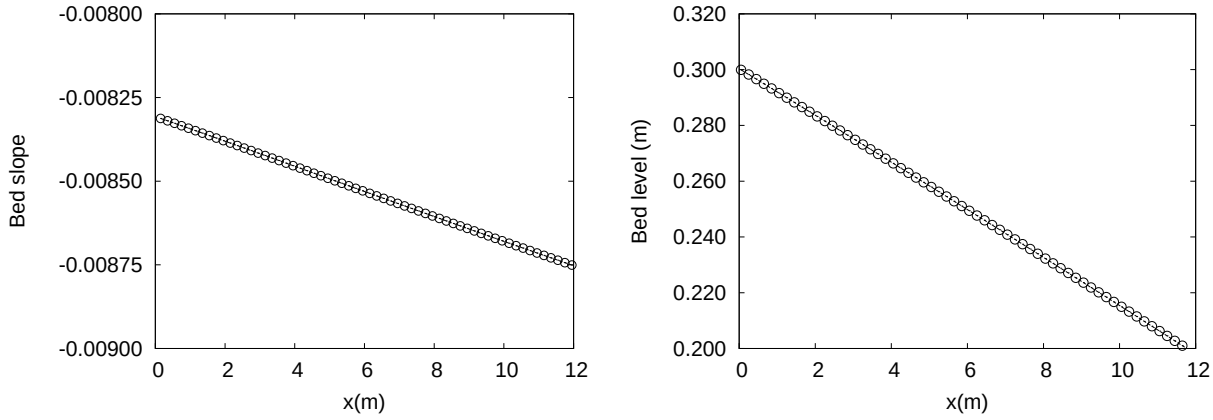

FIG. 11. Test case 4. Bed slope and bed level along the x coordinate

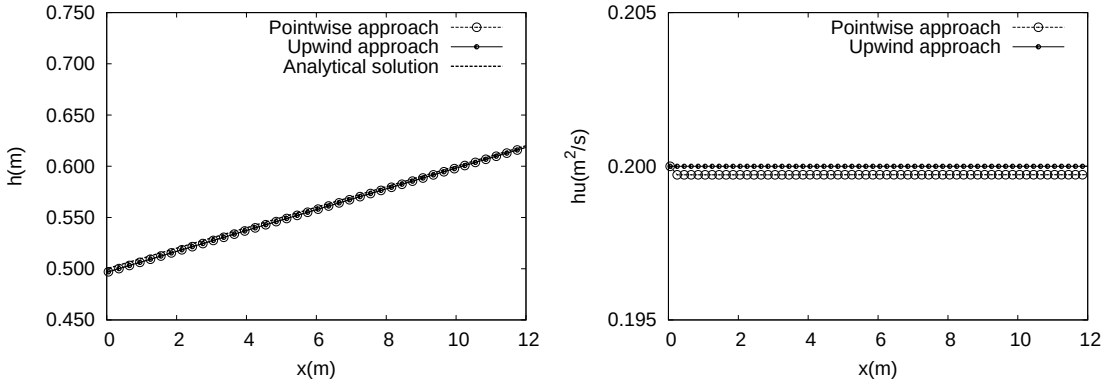

FIG. 12. Test case 4. Numerical solutions for the water level surface and unit discharge flow at $t = 1200$ s when using the pointwise approach and the upwind approach

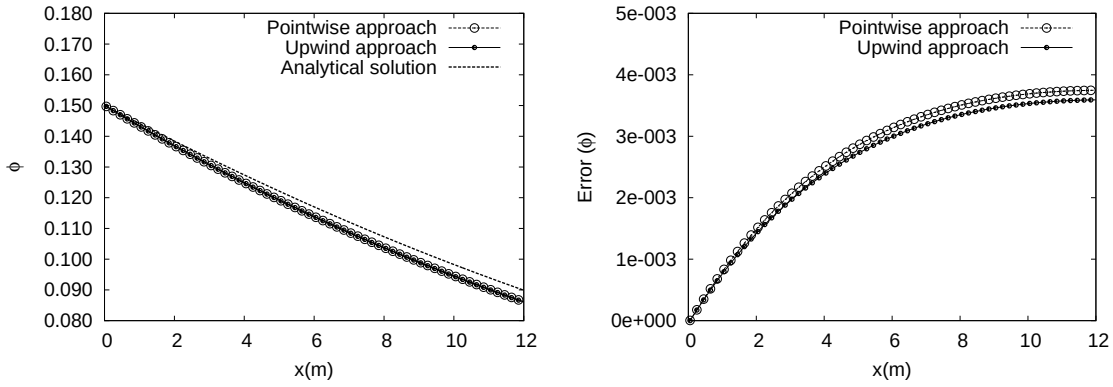

FIG. 13. Test case 4. Sediment concentration and absolute concentration error along the x coordinate at t = 1200 s when using the pointwise approach and the upwind approach

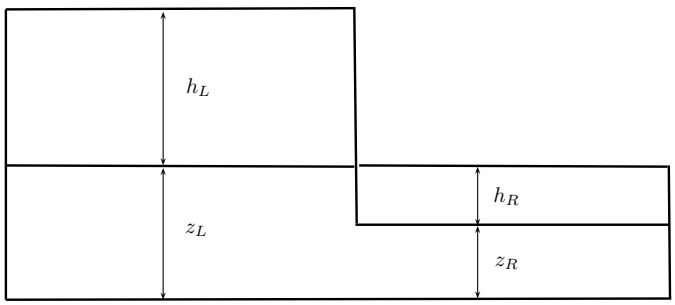

FIG. 14. Sketch of the dam break configuration

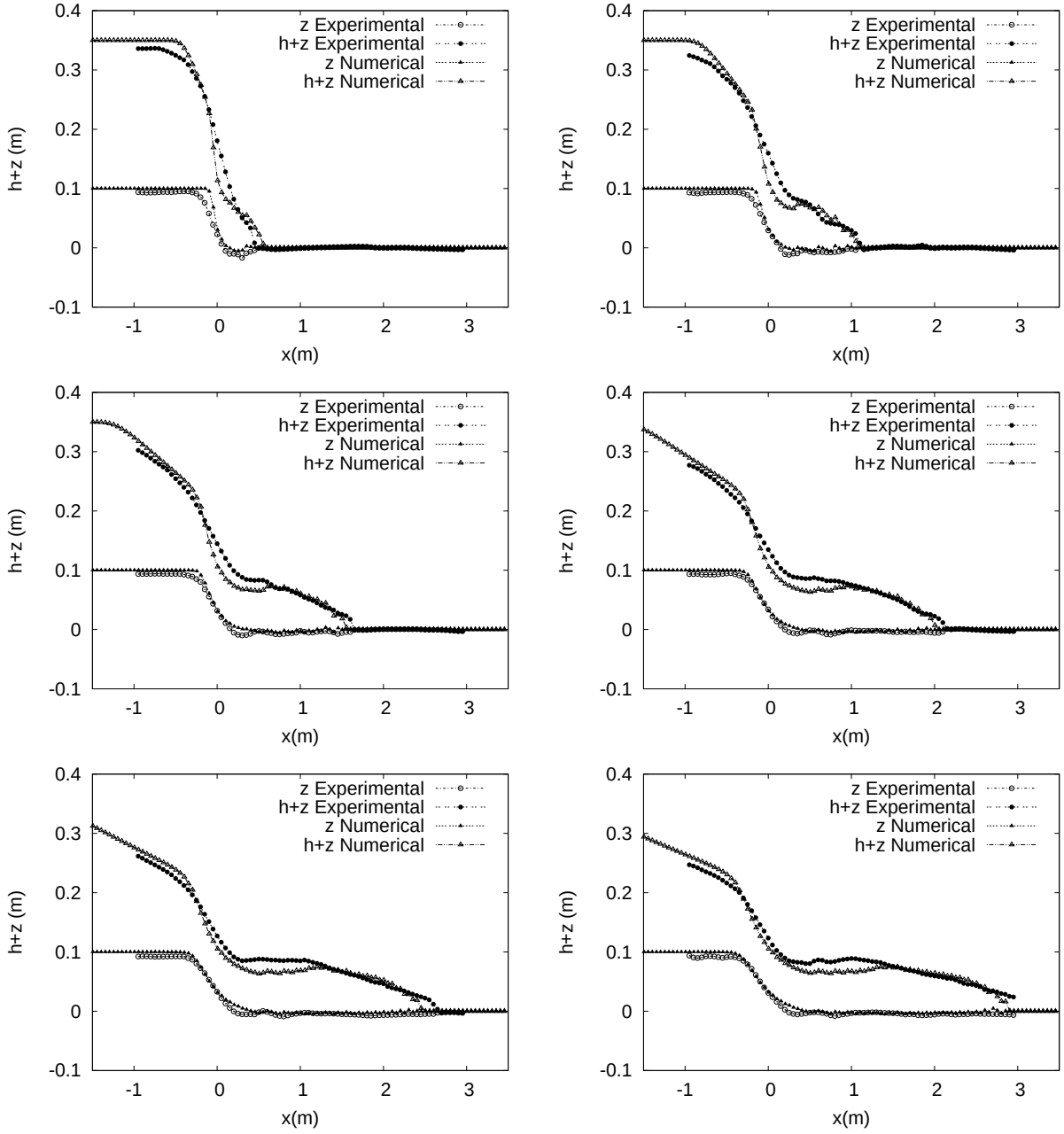

FIG. 15. Test case A. Numerical results and experimental data for the dam break test case A at times $t = 0.025$, 0.050, 0.075, 0.100, 0.125 and 1.5 s, for the measured water level surface, measured bed level surface, computed water level surface, computed bed level surface

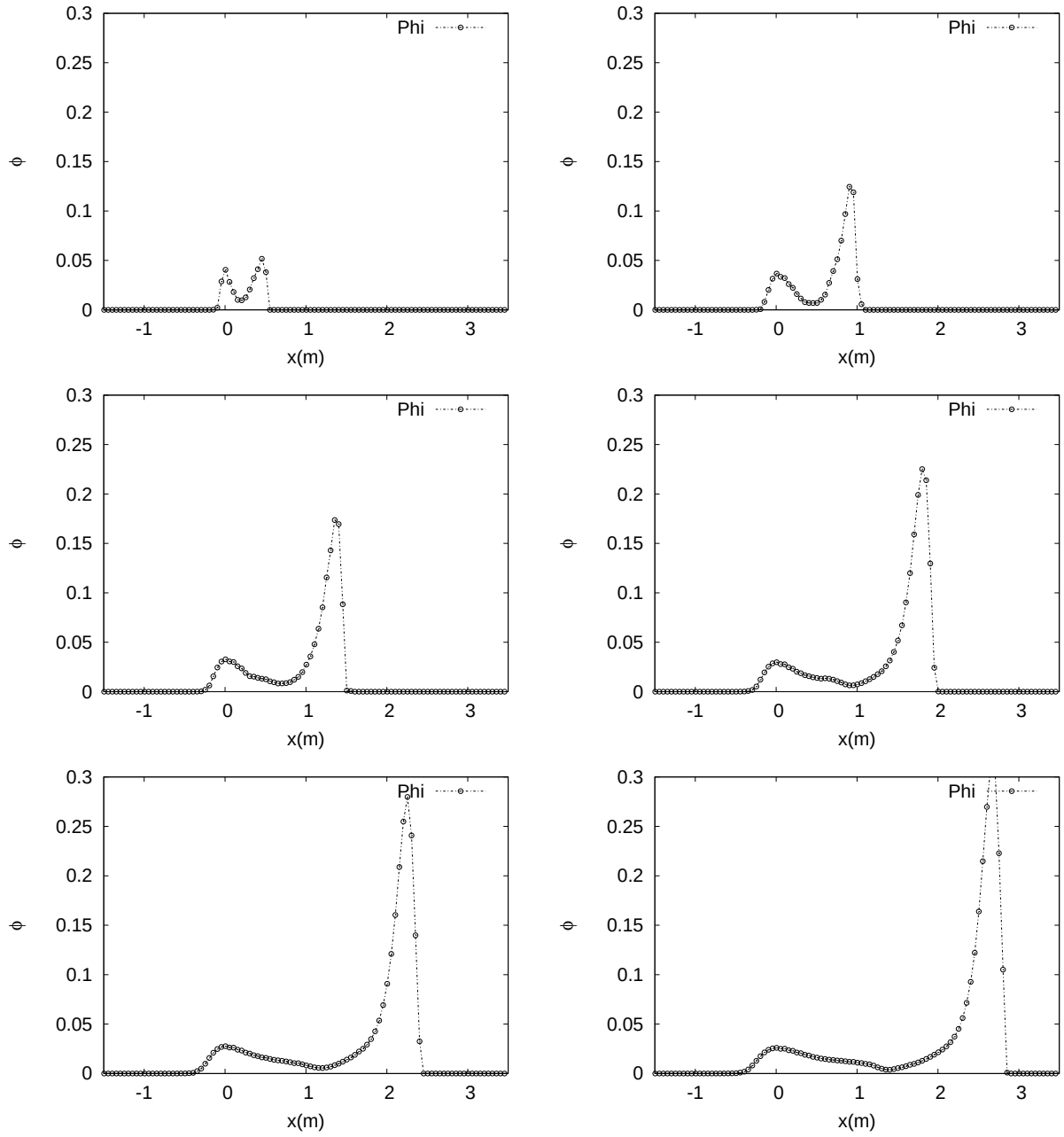

FIG. 16. Test case A. Numerical results for sediment concentration in the dam break test case A at times t = 0.025, 0.050, 0.075, 0.100, 0.125 and 1.5 s

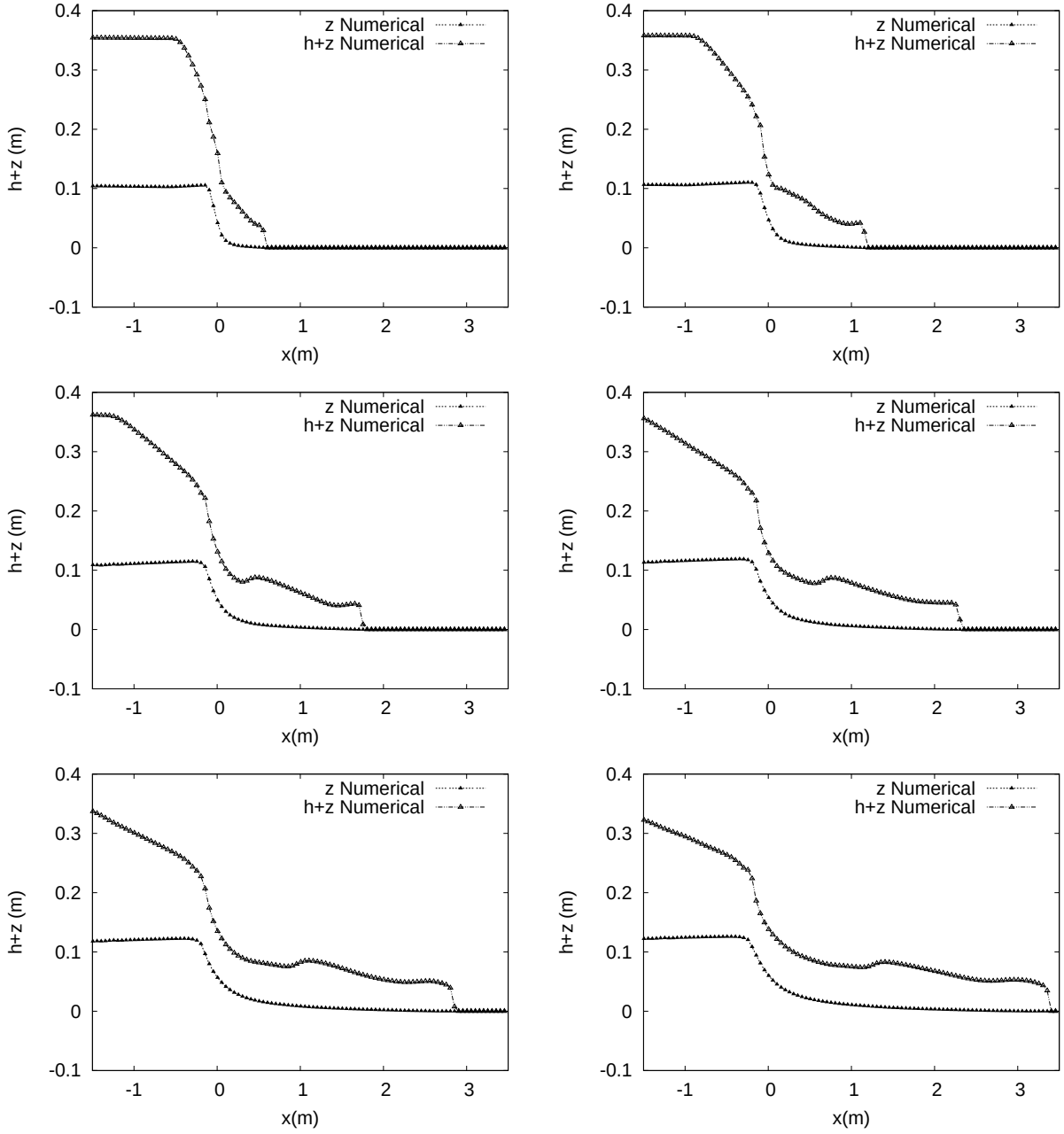

FIG. 17. Test case A. Numerical results assuming $\phi_o = 0.2$ for the dam break test case A at times t = 0.025, 0.050, 0.075, 0.100, 0.125 and 1.5 s, for the computed water level surface and bed level

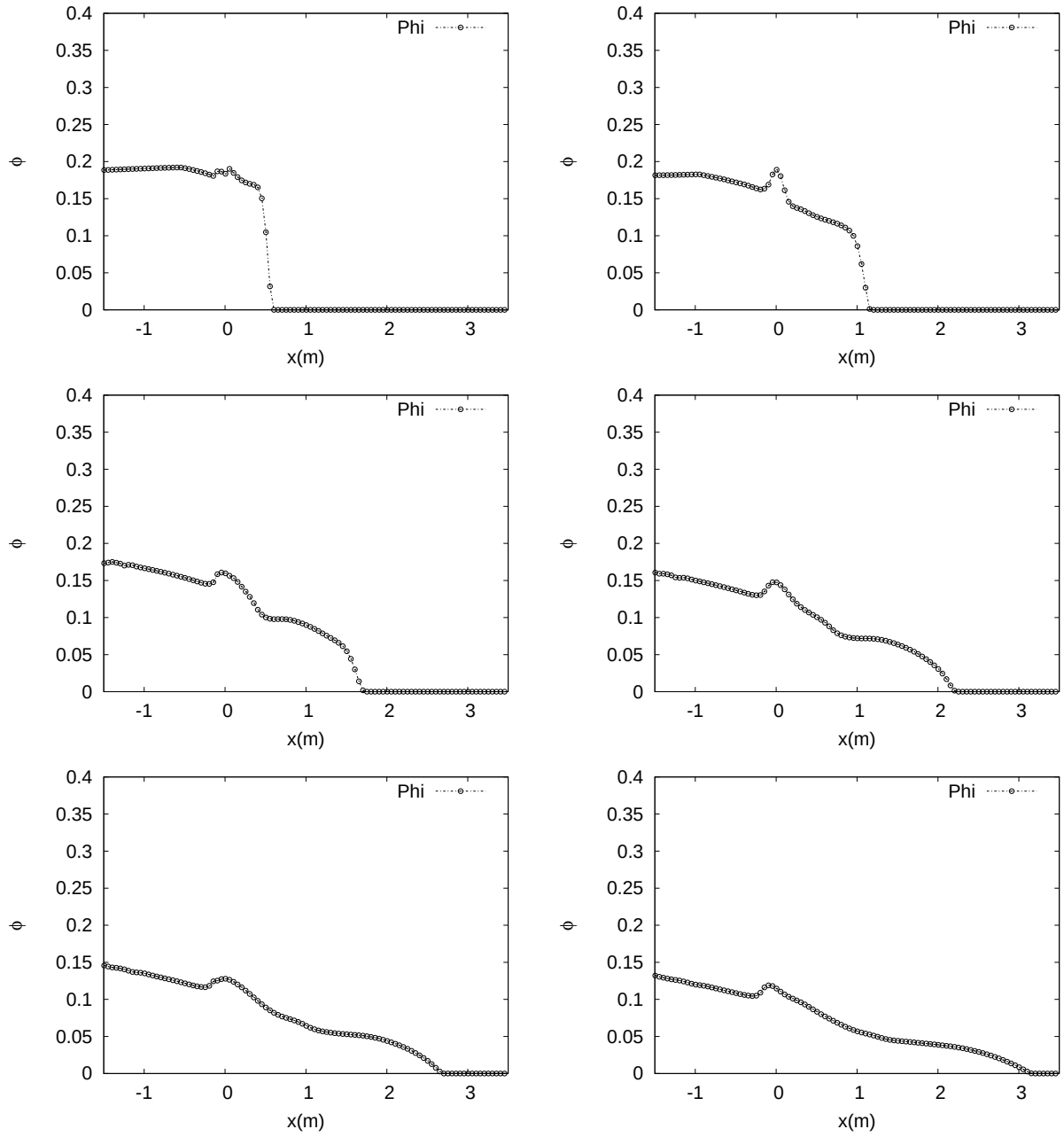

FIG. 18. Test case A. Numerical results assuming $\phi_o = 0.2$ for sediment concentration in the dam break test case A at times t = 0.025, 0.050, 0.075, 0.100, 0.125 and 1.5 s

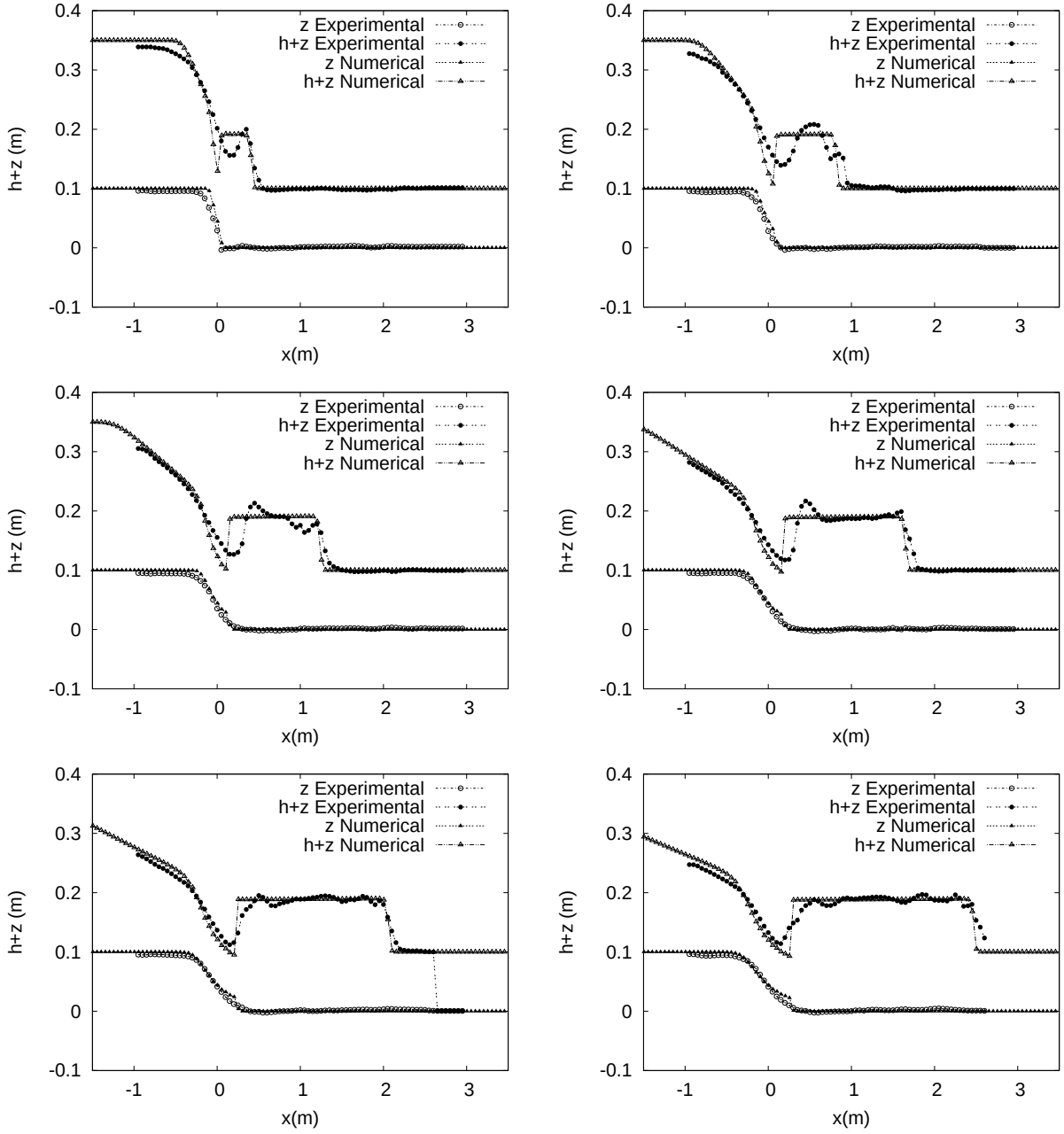

FIG. 19. Test case B. Numerical results and experimental data for the dam break test case B at times t = 0.25, 0.50, 0.75, 1.00, 1.25 and 1.5 s for measured water level surface, measured bed level surface, computed water level surface and computed bed level surface

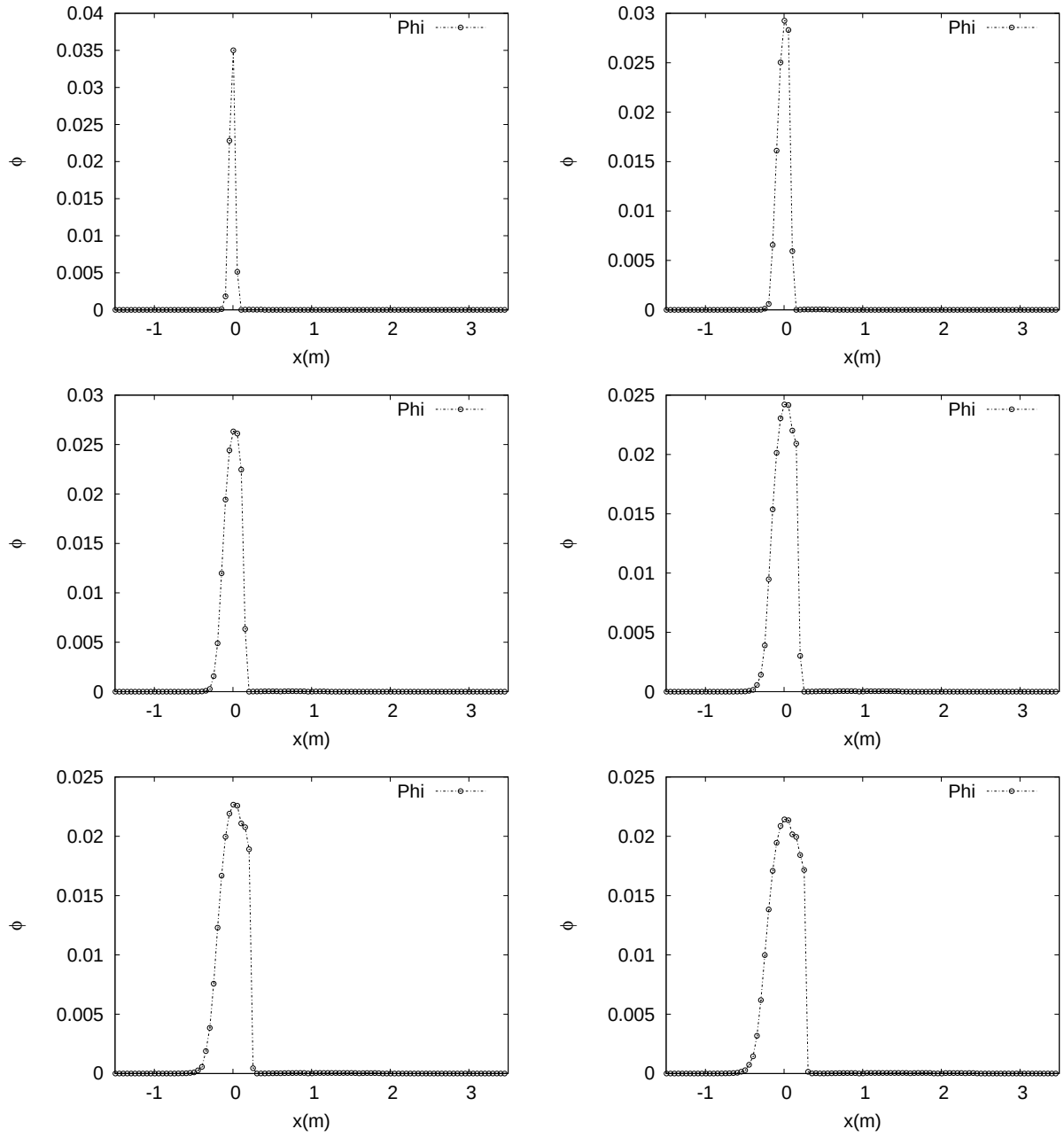

FIG. 20. Test case B. Numerical results for sediment concentration in the dam break test case B at times t = 0.25, 0.50, 0.75, 1.00, 1.25 and 1.5 s